

Entrance channel dependent hot fusion reactions for superheavy element synthesisH. C Manjunatha,^{1,*} N. Sowmya,^{1,2} N. Manjunatha,^{1,3} P. S. Damodara Gupta,^{1,3} L. Seenappa,¹ K. N. Sridhar,⁴ Ganesh T,³ and T. Nandi^{5,†}¹*Department of Physics, Government College for Women, Kolar 563101, Karnataka, India*²*Department of Physics, BMSIT&M, Affiliated to VTU, Bangalore 560064, Karnataka, India*³*Department of Physics, Rajah Serfoji Government College, Thiruchirappalli 620024, India*⁴*Department of Physics, Government First Grade College, Kolar 563101 Karnataka, India*⁵*Inter University Accelerator Centre, Aruna Asaf Ali Marg, JNU New Campus, New Delhi 110067, India*

(Received 23 September 2020; accepted 10 November 2020; published 8 December 2020)

We have studied the compound nucleus probability, the survival probability, and the evaporation residue cross sections for 6645 projectile-target combinations to synthesize the superheavy nuclei with atomic numbers $Z = 110$ – 126 in the light of the entrance channel effects such as mass asymmetry, charge asymmetry, isospin asymmetry, non-compound nuclear fission probability, and Businaro-Gallone mass asymmetry. The role of quasifission in every reaction has also been considered. Decay chains of various superheavy nuclei produced from the reactions are portrayed as well. The most striking results are that the measured evaporation residue cross sections are of the order of picobarns, whereas the proposed reactions can yield up to microbarn cross sections for the superheavy nuclei with $110 \leq Z \leq 126$. We suggest future experiments may utilize these hot fusion reactions to synthesize new elements ($Z > 118$) or to study the properties of the known superheavy nuclei in greater detail. In particular, a proposed reaction containing both projectiles and targets that are naturally abundant, for example, ${}^{82}_{36}\text{Kr} + {}^{232}_{90}\text{Th} \rightarrow {}^{314}_{126} + 0n$, yields evaporation residue cross sections as high as 31 nb. The presently available experimental setup can test the prediction with ease to make a dream come true by putting a footstep into the eighth row of the periodic table.

DOI: [10.1103/PhysRevC.102.064605](https://doi.org/10.1103/PhysRevC.102.064605)**I. INTRODUCTION**

Heavy ion fusion reactions are commonly used in the synthesis of heavy and superheavy nuclei. Superheavy elements up to $Z = 118$ have been synthesized by the hot fusion reactions using actinide targets and ${}^{48}\text{Ca}$ as projectiles [1–4]. However, the production cross sections are extremely small, of the order of picobarns (pb). The hot reactions are used because the elements with atomic numbers $Z = 104$ – 112 are synthesized using the cold fusion reactions [5–7], but the evaporation residue cross sections are found to be decreasing with the increase of the atomic number Z of the superheavy compound nuclei. The cross sections are even lower than 1 pb for $Z > 110$, and thus it is difficult to generate the heavier superheavy nuclei in the cold fusion reactions. Furthermore, no cold fusion reactions can constitute any superheavy elements with $Z \geq 114$.

Several theoretical models have been developed to understand the heavy ion fusion reactions leading to superheavy nuclei formation, such as the macroscopic dynamic model [8,9], the fluctuation-dissipation model [10], nucleon collectivization [11], and the dinuclear system model [12–15]. Furthermore, to investigate the fusion dynamics, isospin de-

pendent quantum molecular dynamics models [15–20] have been extensively used. It is very difficult to get a detailed global picture of the superheavy nucleus formation, as many physical parameters alter the fusion. These include the collision strength, the mass asymmetry, deformation and orientation, the isospin, and the shell structure of the colliding nuclei. Such variables are also heavily entangled, making the influence of a single variable difficult to isolate. The early stage of the collision is the key step in the development of the superheavy elements, where the initial conditions play a major role. This determines the selection of the colliding partners, and the kinetic energy used determines the shape. The colliding partners can break apart, usually after multinucleon transfer, which is referred to as quasifission [21–23]. The character of both the fission and the quasifission processes is expressed by their time scales. The time scale for the quasifission is as short as 10^{-21} s [21–24], whereas the fusion fission can even be longer than 10^{-16} s. Hence, the production cross section of a superheavy element is dependent on the entrance channel conditions because a memory of the entrance channel is often retained in the reactions [25]. Subsequently, Ramamurthy and Kapoor [26] show that the memory of entrance channel K -distribution is also maintained. However, this scenario depends on the fissility of the compound nucleus (CN). For example, the reactions involving less fissile compound nuclei for $A \approx 200$ do not show normally any entrance channel effect [27]. In contrast, compound nuclei of $A \approx 220$

*Corresponding author: manjunathhc@rediffmail.com

†Corresponding author: nanditapan@gmail.com

[28] and $A \approx 230$ [26] show a strong sensitivity for the entrance channel asymmetry with the exit channel. This trend is almost obvious with the actinide [29] and superheavy nuclei [30]. About two decades ago, the entrance channel dynamics and competition between the quasifission and complete fusion processes for various cold fusion reactions have been studied in detail [31]. In this work, we are going to search for certain hot fusion reactions where the quasifission probability is small and thus will be useful for their synthesis and studying the properties of the superheavy elements.

A systematic study of collision energies above the fusion barrier shows that the closed shells in the colliding nuclei have a limited impact on the fusion probability [32]. Nevertheless, the competition between the fusion and quasifission is known to be influenced by the nuclear deformation and orientation at energies around the barrier [33–38]. Earlier workers [39–59] have studied different decay modes in the superheavy region and predicted the possible projectile-target combinations to synthesize the superheavy nuclei. Hence in this article, we study the compound nucleus formation probability, survival probability, and evaporation residue cross sections of the superheavy nuclei with $Z = 110$ –126. In addition, we have investigated the entrance channel effects, such as mass asymmetry, charge asymmetry, isospin asymmetry, non-compound nucleus fission probability (NCNF), and Businaro-Gallone mass asymmetry, on the synthesis of superheavy elements. Furthermore, the roles of quasifission and mean quasifission have also been studied by the analysis of compound nuclear fissility and effective entrance channel fissility. From the study of the entrance channel effects, we have predicted the best possible projectile-target combinations for the synthesis of a few superheavy nuclei.

The present study is organized as follows. The methodology used to study the fusion and evaporation residue cross sections for the synthesis of the superheavy nuclei are given in Sec. II. The analysis of the entrance channel effects, such as mass asymmetry, charge asymmetry, isospin asymmetry, NCNF, and Businaro-Gallone mass asymmetry, and the role of quasifission and mean quasifission in the evaporation residue cross sections and compound nucleus formation probability are discussed in Sec. III. Finally a summary of the present work is given in Sec. IV.

II. THEORETICAL FRAMEWORK

A. Fusion cross section

The fusion reaction is divided into two steps, leading to the synthesis of the superheavy nuclei. The target initially captures the projectile in a dinuclear system and then forms the compound nucleus. Finally, by emitting particles or γ rays it loses its excitation energy and deexcites to its ground state. The total interacting potential barrier for the projectile and the target is expressed as

$$V(R) = V_N(R) + V_C(R), \quad (1)$$

where $V_N(R)$ is the nuclear interaction potential and $V_C(R)$ is the Coulomb interaction potential as given by

$$V_C(R) = \frac{e^2 Z_1 Z_2}{R}. \quad (2)$$

Here $e^2 \approx 1.44$, Z_1 and Z_2 are the atomic number of the projectile and target nuclei, respectively, and R is the separation distance between the centers of target and projectile nuclei. The nuclear interaction potential $V_N(R)$ is the nuclear interaction of the modified Woods-Saxon form by using the Skyrme-energy density functional within the extended Thomas-Fermi approach [60]:

$$V_N(R) = \frac{V_0}{1 + \exp[(R - R_0)/a]}. \quad (3)$$

Here a is the diffuseness parameter and R_0 is the minimum nuclear potential distance:

$$R_0 = r_0(A_1^{1/3} + A_2^{1/3}) - b. \quad (4)$$

V_0 in Eq. (3) is the potential height at $R = R_0$ [61] and it is given by

$$V_0 = u_0[1 + \kappa(I_1 + I_2)] \frac{A_1^{1/3} A_2^{1/3}}{A_1^{1/3} + A_2^{1/3}}. \quad (5)$$

Here I_i is the reduced isospin and it is expressed in terms of the neutron number N_i , the proton number Z_i , and the mass number A_i as $I_i = (N_i - Z_i)/A_i$, where $i = 1$ and 2 for projectile and target nuclei, respectively. Values of the five parameters for the least-square fitting of $V_N(R)$ are taken as $r_0 = 1.183$ fm, $b = 1.37$ fm, $u_0 = -46.07$ MeV, $\kappa = -0.4734$, and $a = 0.75$ fm⁻² [60]. With these parameters, the relative deviation achieved with the Skyrme energy-density functional is minimized. The nuclear interaction is assumed to be in the Gaussian form; moreover, the empirical barrier (B) distribution function $D(B)$ is the superposition of two Gaussian functions as under

$$D_1(B) = \frac{\sqrt{\gamma}}{2\sqrt{\pi}b_1} \exp\left[-\gamma \frac{(B - B_1)^2}{(2b_1)^2}\right] \quad (6)$$

and

$$D_2(B) = \frac{\sqrt{\gamma}}{2\sqrt{\pi}b_2} \exp\left[-\gamma \frac{(B - B_2)^2}{(2b_2)^2}\right], \quad (7)$$

with

$$B_1 = B_c + b_1, \quad (8)$$

$$B_2 = B_c + b_2, \quad (9)$$

$$b_1 = \frac{1}{4}(B_0 - B_c), \quad (10)$$

$$b_2 = \frac{1}{2}(B_0 - B_c). \quad (11)$$

Here, B_0 and B_c are the barrier height and the effective barrier height, and they are related as $B_c = fB_0$ with the reduction factor $f = 0.926$. The parameter γ in Eqs. (6) and (7) is the factor that involves the structure effects whose value is greater or equal to 0.5. For the fusion reactions at energies near or above the barrier, $\gamma = 1$ [62]. The fusion excitation function [62,63] is taken as

$$\sigma_{\text{fus}}(E_{\text{cm}}) = \min[\sigma_1(E_{\text{cm}}), \sigma_{\text{avr}}(E_{\text{cm}})], \quad (12)$$

with

$$\sigma_1(E_{\text{cm}}) = \int_0^\infty D_1(B) \sigma_{\text{fus}}^{\text{Wong}}(E_{\text{cm}}, B) dB \quad (13)$$

and

$$\sigma_{\text{avr}}(E_{\text{cm}}) = \int_0^\infty \left[\frac{D_1(B) + D_2(B)}{2} \right] \sigma_{\text{fus}}^{\text{Wong}}(E_{\text{cm}}, B) dB, \quad (14)$$

where $\sigma_{\text{fus}}^{\text{Wong}}$ is the fusion cross section [64] for two deformed and oriented nuclei, colliding with E_{cm} is

$$\sigma_{\text{fus}}^{\text{Wong}}(E_{\text{cm}}, B) = \frac{\hbar\omega R_{\text{fus}}^2}{2E_{\text{cm}}} \ln \left(1 + \exp \left[\frac{2\pi}{\hbar\omega} (E_{\text{cm}} - B_0) \right] \right). \quad (15)$$

Here E_{cm} , B_0 , R_{fus} , and $\hbar\omega$ are the center-of-mass energy, the barrier height, the barrier radius, and the barrier curvature, respectively. The effect of the angular momentum is already included in the Wong's formula by the assumption that the barrier position and the barrier curvature do not change with the angular momentum.

B. Evaporation residue cross section

The evaporation residue cross section of a super heavy element [41,45] with subsequent emission of light particles is expressed as

$$\sigma_{\text{ER}}^{xn} = \frac{\pi}{k^2} \sum_{\ell=0}^{\infty} (2\ell + 1) T(E, \ell) P_{\text{CN}}(E^*, \ell) P_{\text{sur}}^{xn}(E^*, \ell), \quad (16)$$

where $T(E, \ell)$ is the probability that the particle will pass through the potential barrier; it is a function of the center-of-mass energy E and the angular momentum $\ell\hbar$; and $P_{\text{CN}}(E^*, \ell)$ is the probability that the CN reaches the equilibrium configuration as a function of the excitation energy E^* and ℓ . The survival probability $P_{\text{sur}}^{xn}(E^*, \ell)$ is the probability that the fused system emits x number of neutrons followed by a sequence of α decay from the residue, which is given by

$$P_{\text{sur}}^{xn} = P_{xn}(E^*) \prod_{i=1}^{i_{\text{max}}=x} \left(\frac{\Gamma_n}{\Gamma_n + \Gamma_f} \right)_{i, E^*}. \quad (17)$$

The survival probabilities are evaluated using a statistical evaporation code called HIVAP [65]. The HIVAP code uses standard evaporation theory and includes the competition of γ -ray, neutron, proton and α -particle emission and fission using an angular momentum and level density formula [65]. P_{xn} is the probability of realization of the evaporation sequence as given by [11]

$$P_{xn} = \int_0^{E_0^* - B_n(1)} \frac{\Gamma_b}{\Gamma_{\text{tot}}}(E_0^*, I_0) W_n(E_0^*, e_1) de_1 \int_0^{E_1^* - B_n(2)} \frac{\Gamma_n}{\Gamma_{\text{tot}}}(E_1^*, I_1) W_n(E_1^*, e_2) de_2 \\ \times \int_0^{E_{n-1}^* - B_n(x)} \frac{\Gamma_n}{\Gamma_{\text{tot}}}(E_{x-1}^*, I_{x-1}) W_n(E_{x-1}^*, e_x) \times \prod_{i=1}^N \frac{\Gamma_\gamma}{\Gamma_{\text{tot}}}(E_i^*, I_i) de_x. \quad (18)$$

Here $B_n(i)$ is the binding energy and e_i is the kinetic energy of the i th evaporated neutron. $W_n(E^*, e) = C_n \sqrt{e} \exp[-e/T(E^*)]$ is the probability for the evaporated light particles to have energy e . C_n is the normalized coefficient and it is determined from the equation $\int_0^{E^* - B_n} W_n(E^*, e) de = 1$.

C. Decay widths

The compound nucleus is formed in the excited state; it can decay through the different channels, such as neutrons (n), protons (p), α particles (${}^4\text{He}$), and γ photons, and fission into heavy fragments. The decay width of the particle emission can be calculated as

$$\Gamma_{C \rightarrow B+b}(E^*, J) = \frac{2S_b + 1}{2\pi \rho_c(E^*, J)} \int_0^{E^* - B_b} \sum_{\ell} T_{\ell}(e_b) \sum_{I=|J-1|}^{I=J+1} \rho_B(E^* - B_b - e_b, I) de_b, \quad (19)$$

where S_b is spin of the emitted particles such as neutrons, protons, or α particles. B_b is the corresponding binding energy. $T_{\ell}(e)$ is the probability of the particle passing through the potential barrier with the kinetic energy e of the emitting particle [66], and $T_{\ell}(e)$ for the charged particles is expressed as

$$T_{\ell}(e) = \frac{P(e)}{\left\{ 1 + \exp \left[\frac{2\pi}{\hbar\omega} \left(V_c + \frac{\hbar^2 \ell(\ell+1)}{2\mu R^2} - e \right) \right] \right\}}, \quad (20)$$

where μ is the reduced mass of the particle and the radius is given by $R = r_0 A^{1/3} + 2$ fm. $P(e)$ in Eq. (20) is given by

$$P(e) = \frac{\sqrt[4]{\frac{e}{e+40}}}{\left(1 + \sqrt{\frac{e}{e+40}} \right)^2}. \quad (21)$$

The barrier height (V_c) and the width $\hbar\omega$ for proton decay can be calculated in MeV units as

$$V_c = 0.106 - 0.9 + 0.02(Z + N^* - A) \text{ and} \\ \hbar\omega = 6.2 + 0.04(Z - 20), \quad (22)$$

and for α particles they can be calculated as

$$V_c = 0.195(Z - 2) + 4.5 + 0.02(Z + N^* - A) \text{ and} \\ \hbar\omega = 6.03 + 0.016(Z - 100). \quad (23)$$

$$T_\ell(e) = P(e) \exp \left\{ -2\sqrt{\frac{2e\mu}{\hbar^2}} \left[\rho^2 - R^2 + \rho \log \left(\frac{\rho + \sqrt{\rho^2 - R^2}}{R} \right) \right] \right\}, \text{ where } \rho = \sqrt{\frac{\hbar^2 \ell(\ell + 1)}{2e\mu}}. \quad (24)$$

The fission width is studied using the following expression:

$$\Gamma_{\text{fis}}(E^*, J) = \frac{K_{\text{Kramers}}}{2\pi \rho_c(E^*, J)} \int_0^{E^*} T_{\text{fis}}(e, J) \rho_C^{\text{s,p}}(E^* - e, J) de, \quad (25)$$

where $T_{\text{fis}}(e, J)$ is the fission barrier penetrability,

$$T_{\text{fis}}(e, J) = \frac{1}{1 + \exp \left[-\frac{2\pi}{\hbar\omega_{\text{s,p}}} (e - B_{\text{fis}}(E^*)) \right]}, \quad (26)$$

and K_{Kramers} is the Kramers factor, given by

$$K_{\text{Kramers}} = \frac{\hbar \omega_{\text{g,s}}}{T \omega_{\text{s,p}}} \left(\sqrt{\omega_{\text{s,p}}^2 + \zeta^2/4} - \zeta/2 \right). \quad (27)$$

Here the nuclear temperature $T = \sqrt{U/a}$ (U is defined below), ζ is the viscosity parameter, and $\hbar\omega_{\text{g,s}}$ and $\hbar\omega_{\text{s,p}}$ are the potential curvatures at the ground state and the saddle point, respectively [67]. The fission barrier (B_{fis}) has been studied early [68]. The level density [60] in Eq. (25) is expressed as [69]

$$\rho(J, E^*) = \frac{1}{24} \left(\frac{\hbar^2}{2I} \right)^{3/2} (2J + 1) a^{1/2} U_J^{-2} \exp[2(aU_J)^{1/2}] \quad (28)$$

and

$$U_J = E^* - E_r(J). \quad (29)$$

Here $E_r(J)$ is the yrast energy and it is expressed as

$$E_r(J) = J(J + 1)\hbar^2/2I, \quad (30)$$

where I and J are the moment of inertia and the angular momentum, respectively, $\hbar = \frac{h}{2\pi}$, and a is the level density parameter expressed as

$$a = \tilde{a}[1 + f(E^*)S/E^*], \quad (31)$$

where S and E^* are the shell correction and the excitation energy, respectively, and

$$f(E^*) = 1 - \exp(-E^*/E_d), \quad (32)$$

where $E_d = 1.5$ MeV is the small shell damping energy. The smooth shell independent level-density parameter \tilde{a} is given by

$$\tilde{a} = 0.04543r_a^3A + 0.1355r_a^2A^{2/3}B_s + 0.1426r_aA^{1/3}B_k, \quad (33)$$

where A is the mass number of the compound nuclei and r_a is the separation distance between the fissioning nuclei. The level density parameter includes terms such as surface (B_s)

and volume and curvature factors (B_k) as defined in the droplet model [69]. For the evaporation channel, $B_s = B_k = 1$. The ratio of \tilde{a}_f/\tilde{a}_n , i.e., the level density parameter for the fission channel (\tilde{a}_f) to the level density parameter for the neutron channel (\tilde{a}_n), is greater than 1 and it decreases to 1 with the fissility parameter increases. When the compound nucleus is formed in the excited state, it decays into heavy fragments through the various channels, such as neutrons, protons, or α particles, through fission. Using the standard HIVAP code, the fission barrier at zero angular momentum is studied by

$$B_f = B_f^{\text{Mac}} - S. \quad (34)$$

Here B_f^{Mac} is the macroscopic barrier described by the liquid drop model [64,70,71], and S is the shell correction and it is estimated by taking the the difference between the experimental mass and the liquid drop mass, $S = M_{\text{exp}} - M_{\text{LD}}$. In the HIVAP code, the M_{LD} is determined by using the parameter set of Myers and Swiatecki [72] and the experimental mass values were taken from the available literature [65].

III. RESULTS AND DISCUSSIONS

A. Entrance channel effects on cross sections

We have studied the compound nucleus probability, the survival probability, and the evaporation residue cross sections for the 6645 projectile-target combinations to synthesize the superheavy nuclei with atomic numbers $110 < Z < 126$; the range of atomic numbers and the mass numbers of the projectiles and targets considered in the present study are given in Table I. Further, we have extended our study to see the entrance channel characteristics of the fusion dynamics to show the relative importance of the influence on the projectile and target nuclei. In particular, we show how their contributions vary with the entrance channel characteristics such as mass asymmetry, charge asymmetry, isospin asymmetry, non-compound nucleus fission probability, Businaro-Gallone (BG) mass asymmetry α_{BG} , and quasifission and mean quasifission. This will supposedly give us an insight into the mechanism and an idea of the choice of the projectile and target combinations during the synthesis of the superheavy nuclei.

1. Mass and charge asymmetry

From the literature [26,29,73] it is observed that the mass asymmetry $\eta = |(A_1 - A_2)/(A_1 + A_2)|$ and the charge asymmetry $\alpha_z = |(Z_1 - Z_2)/(Z_1 + Z_2)|$ of the entrance channel play a major role in the dynamic evolution of a dinuclear system, which leads to the formation of a compound nucleus.

TABLE I. The range of the projectile-target combinations studied to synthesize the superheavy elements with $Z = 110$ – 126 along with their atomic and mass number ranges.

SHN	No. of reactions studied	Range of projectile		Range of target	
		Z	A	Z	A
110	556	$16 < Z < 26$	$35 < A < 55$	$84 < Z < 94$	$210 < A < 246$
111	267	$13 < Z < 23$	$26 < A < 50$	$88 < Z < 98$	$226 < A < 246$
112	288	$14 < Z < 40$	$28 < A < 96$	$72 < Z < 98$	$182 < A < 249$
113	266	$15 < Z < 20$	$32 < A < 48$	$93 < Z < 98$	$239 < A < 250$
114	397	$32 < Z < 40$	$70 < A < 96$	$74 < Z < 82$	$182 < A < 203$
115	681	$19 < Z < 21$	$39 < A < 48$	$94 < Z < 96$	$240 < A < 244$
116	728	$19 < Z < 32$	$40 < A < 70$	$84 < Z < 97$	$206 < A < 254$
117	488	$5 < Z < 33$	$10 < A < 75$	$84 < Z < 112$	$222 < A < 279$
118	671	$20 < Z < 34$	$40 < A < 82$	$84 < Z < 98$	$219 < A < 252$
119	123	$22 < Z < 31$	$44 < A < 72$	$88 < Z < 97$	$227 < A < 248$
120	382	$30 < Z < 42$	$72 < A < 95$	$78 < Z < 90$	$190 < A < 232$
121	197	$23 < Z < 35$	$48 < A < 82$	$86 < Z < 98$	$222 < A < 251$
122	323	$8 < Z < 38$	$17 < A < 89$	$84 < Z < 114$	$225 < A < 290$
123	582	$25 < Z < 34$	$52 < A < 82$	$89 < Z < 98$	$236 < A < 251$
124	202	$12 < Z < 40$	$28 < A < 96$	$84 < Z < 112$	$222 < A < 285$
125	373	$27 < Z < 37$	$56 < A < 87$	$88 < Z < 98$	$228 < A < 247$
126	121	$13 < Z < 40$	$27 < A < 94$	$86 < Z < 113$	$230 < A < 280$

We have studied the mass asymmetry and charge asymmetry for the superheavy nuclei with $Z = 110$ – 126 with respect to evaporation residue cross sections. Figure 1 shows the variation of mass asymmetry with that of the evaporation residue cross sections for the combination of even (Z)-even (N) nuclei. From the figure it can be clearly observed that as the mass asymmetry decreases for the projectile-target combination the corresponding evaporation residue cross section also decreases in all the cases. A similar trend is also observed for even (Z)-odd (N), odd (Z)-odd (N), and odd (Z)-even (N) compound nuclei. Therefore, it is clear from the figure that mass asymmetry plays a major role in the formation of the compound nuclei. If η is large, then the probability of compound nucleus formation is also large. Note that η and α_Z vary back to back, and hence the σ_{ER} varies similarly with the α_Z also, as evident from Table II.

2. Businaro-Gallone mass asymmetry

The Businaro-Gallone critical mass asymmetry parameter is expressed as

$$\alpha_{BG} = \begin{cases} 0 & \text{for } \chi < \chi_{BG}, \\ 1.12 \sqrt{\frac{(\chi - \chi_{BG})}{(\chi - \chi_{BG}) + 0.24}} & \text{for } \chi > \chi_{BG}, \end{cases} \quad (35)$$

where the fissility parameter $\chi = (\frac{Z^2}{A})/50.8831 - 1.7826(\frac{N-Z}{A})^2$ and $\chi_{BG} = 0.396$. The Businaro-Gallone critical mass asymmetry plays a strong role in determining the path of equilibrium dynamics [79]. The projectile-target combinations with α_{BG} values less than the Businaro-Gallone critical mass asymmetry value (α_{BG}^C) of 0.9 exhibit the anomalous fission fragment anisotropies at the above-barrier energies [80]. The evaporation residue cross sections (σ_{ER}) with the Businaro-Gallone mass asymmetry (α_{BG}) portrayed in Fig. 2 show that as the α_{BG} increases the corresponding

σ_{ER} also increases. It can also be noticed from Table II that the values of α_{BG} for the projectile-target combinations used here are >1 . This is a common fact for all the cold fusion reactions as well as the hot fusion reactions used to synthesize the superheavy elements. Hence, very importantly, the projectile-target combinations discussed here will not display any anomalous fission fragment anisotropy, rather these systems will exhibit the expected fission-fragment anisotropy at the above-barrier energies [79].

3. Isospin asymmetry

The isospin asymmetry is the difference in the N/Z ratios of the projectile and the target and it is expressed as

$$\Delta\left(\frac{N}{Z}\right) = \left| \left(\frac{N}{Z}\right)_P - \left(\frac{N}{Z}\right)_T \right|. \quad (36)$$

The influence of isospin asymmetry as a function of evaporation residue cross sections for the synthesis of superheavy nuclei with $Z = 120$ is shown in Fig. 3. As the isospin asymmetry decreases there is a decrease in the evaporation residue cross section also.

4. Coulomb interaction parameter

The Coulomb interaction parameter between the two nuclei is defined as

$$z = \frac{Z_1 Z_2}{A_1^{1/3} + A_2^{1/3}}. \quad (37)$$

We have studied the compound nucleus probability P_{CN} as a function of z and the variation is presented in Fig. 4. The present study also parametrizes the probability of compound nuclei formation in terms of z . The best fitted equation for the compound nucleus probability is considered such that the residual sum of the squares must be nearly equal to 1 and the

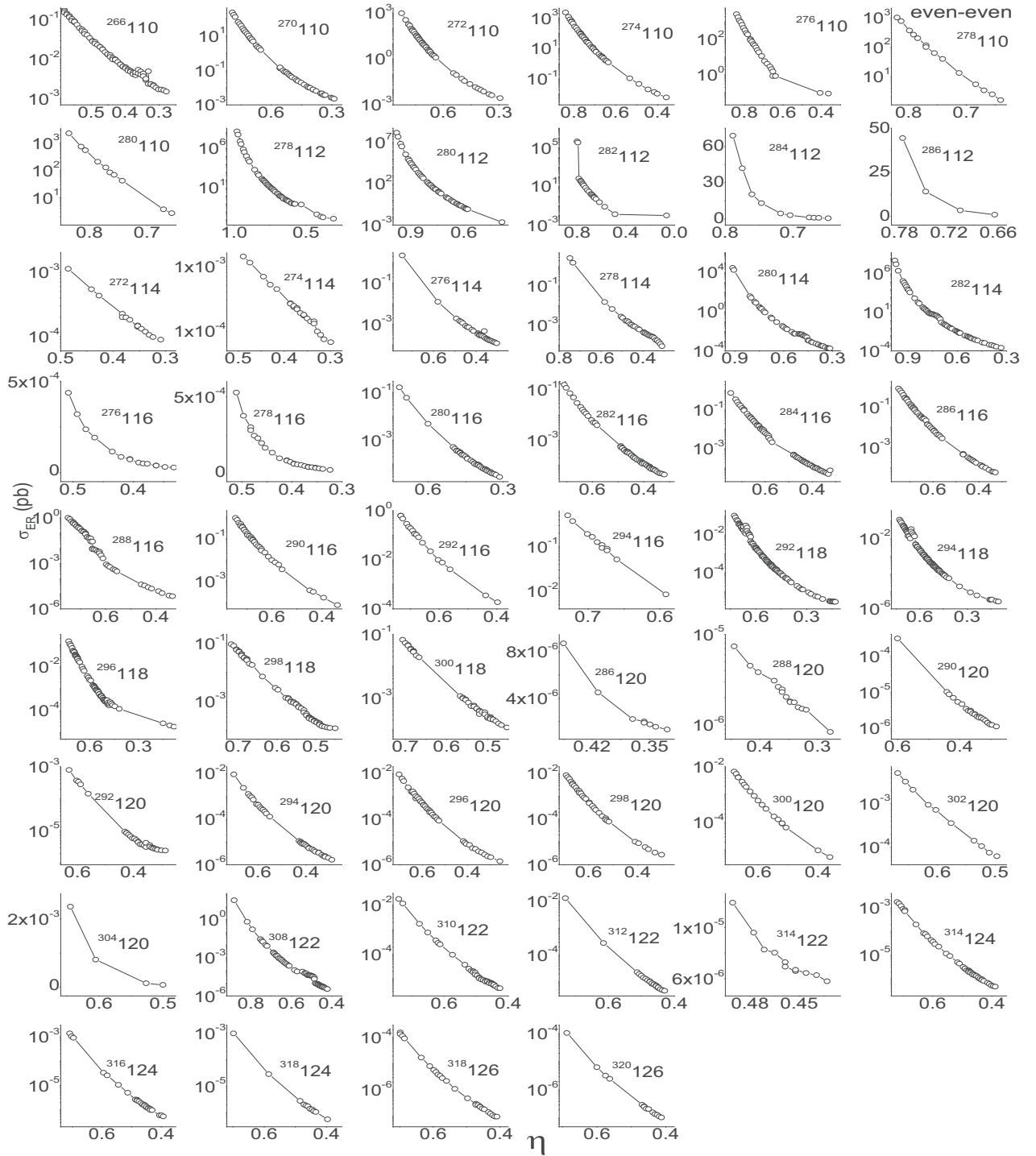


FIG. 1. Variation of the evaporation residue cross sections with the mass asymmetry parameter (η) for the even-even superheavy nuclei with $Z = 110$ – 126 .

constructed equation is as follows:

$$P_{CN} = 0.9145^z \quad (38)$$

As the interaction parameter increases for the different projectile-target combinations, the P_{CN} gradually decreases, which in turn shows the effect of z on the different projectile-target combinations. Figure 5 gives the variation of the fusion barrier with z . We have exercised regressions to fit the best

equation for the fusion barrier in terms of z :

$$V_B(\text{MeV}) = 0.6544 \times z^{1.093}. \quad (39)$$

Figure 6 represents the variation of the evaporation residue cross section in pb with z for the superheavy region $Z = 110$ – 126 . We have also fitted the evaporation residue cross sections

TABLE II. Dependence of the evaporation residue cross section on the entrance channel effects such as the mass asymmetry (η), charge asymmetry (α_z), isospin asymmetry [$\Delta(N/Z)$], Coulomb charge (Z_1Z_2), Coulomb interaction parameter (z), mean fissility χ_m , and Businaro-Gallone mass asymmetry (α_{BG}) for the synthesis of the superheavy nuclei $Z = 110$ –126.

Reaction	Z_1Z_2	E_{cm}	E_{lab}	η	α_z	$\Delta(N/Z)$	z	χ_m	α_{BG}	σ_{ER}^{Theo}	σ_{ER}^{Expt}	Remark
$^{62}_{28}\text{Ni} + ^{208}_{82}\text{Pb} \rightarrow ^{269}_{110}\text{Ds} + 1n$	2296	261.37	339.29	0.54	0.49	0.32	232.32	0.86	1.05	4 pb	$3.5^{+2.7}_{-1.8}$ pb [5]	Used
$^{25}_{12}\text{Mg} + ^{251}_{98}\text{Cf} \rightarrow ^{272}_{110}\text{Ds} + 4n$	1176	153.16	168.41	0.82	0.78	0.48	127.38	0.67	1.06	1.19 nb		Prop.
$^{26}_{13}\text{Al} + ^{253}_{97}\text{Bk} \rightarrow ^{274}_{110}\text{Ds} + 5n$	1261	166.45	183.55	0.81	0.76	0.61	135.78	0.70	1.06	0.119 nb		Prop.
$^{26}_{13}\text{Al} + ^{249}_{97}\text{Bk} \rightarrow ^{270}_{110}\text{Ds} + 5n$	1261	172.45	190.45	0.81	0.76	0.57	136.27	0.70	1.06	0.17 nb		Prop.
$^{64}_{28}\text{Ni} + ^{209}_{83}\text{Bi} \rightarrow ^{272}_{111}\text{Rg} + 1n$	2324	263.43	344.1	0.53	0.50	0.23	233.	0.86	1.05	13 pb	$3.5^{+4.6}_{-2.3}$ pb [74]	Used
$^{48}_{21}\text{Sc} + ^{234}_{90}\text{Th} \rightarrow ^{279}_{111}\text{Rg} + 3n$	1890	209.87	252.92	0.66	0.62	0.31	192.93	0.79	1.06	0.181 nb		Prop.
$^{33}_{15}\text{P} + ^{248}_{96}\text{Cm} \rightarrow ^{277}_{111}\text{Rg} + 4n$	1440	180.16	204.13	0.77	0.73	0.38	151.73	0.72	1.06	0.225 nb		Prop.
$^{37}_{17}\text{Cl} + ^{242}_{94}\text{Pu} \rightarrow ^{275}_{111}\text{Rg} + 4n$	1598	198.16	228.45	0.73	0.69	0.40	167.09	0.75	1.05	0.456 nb		Prop.
$^{40}_{19}\text{K} + ^{238}_{92}\text{U} \rightarrow ^{273}_{111}\text{Rg} + 5n$	1748	220.45	257.49	0.71	0.66	0.48	181.76	0.78	1.05	0.225 nb		Prop.
$^{70}_{30}\text{Zn} + ^{208}_{82}\text{Pb} \rightarrow ^{277}_{112}\text{Cn} + 1n$	2460	276.45	369.48	0.49	0.46	0.20	244.86	0.8	1.04	0.47 pb	$0.5^{+1.1}_{-0.4}$ pb [74]	Used
$^{42}_{18}\text{Ar} + ^{242}_{94}\text{Pu} \rightarrow ^{281}_{112}\text{Cn} + 3n$	1692	191.87	225.17	0.70	0.68	0.24	174.29	0.75	1.05	0.321 nb		Prop.
$^{47}_{20}\text{Ca} + ^{238}_{92}\text{U} \rightarrow ^{282}_{112}\text{Cn} + 3n$	1840	211.87	253.71	0.67	0.64	0.24	187.64	0.77	1.05	0.944 nb		Prop.
$^{33}_{15}\text{P} + ^{249}_{97}\text{Bk} \rightarrow ^{278}_{112}\text{Cn} + 4n$	1455	182.16	206.30	0.77	0.73	0.37	153.18	0.72	1.05	0.15 nb		Prop.
$^{70}_{30}\text{Zn} + ^{209}_{83}\text{Bi} \rightarrow ^{278}_{113}\text{Nh} + 1n$	2490	279.76	373.47	0.49	0.46	0.18	247.61	0.87	1.04	0.53 pb	55^{+150}_{-45} fb [75]	Used
$^{31}_{15}\text{P} + ^{254}_{98}\text{Cf} \rightarrow ^{281}_{113}\text{Nh} + 4n$	1274	181.16	203.27	0.78	0.73	0.53	155.15	0.74	1.05	0.372 nb		Prop.
$^{37}_{17}\text{Cl} + ^{250}_{96}\text{Cm} \rightarrow ^{283}_{113}\text{Nh} + 4n$	1632	198.16	227.48	0.74	0.70	0.43	169.44	0.76	1.05	2.16 nb		Prop.
$^{32}_{15}\text{P} + ^{252}_{98}\text{Cf} \rightarrow ^{280}_{113}\text{Nh} + 4n$	1470	183.16	206.41	0.77	0.73	0.44	154.88	0.73	1.05	0.613 nb		Prop.
$^{33}_{15}\text{P} + ^{253}_{98}\text{Cf} \rightarrow ^{282}_{113}\text{Nh} + 4n$	1470	183.16	207.05	0.77	0.73	0.38	154.21	0.72	1.05	3.93 nb		Prop.
$^{33}_{16}\text{S} + ^{249}_{97}\text{Bk} \rightarrow ^{277}_{113}\text{Nh} + 5n$	1552	203.45	230.41	0.77	0.72	0.50	163.39	0.75	1.05	0.125 nb		Prop.
$^{48}_{20}\text{Ca} + ^{244}_{94}\text{Pu} \rightarrow ^{289}_{114}\text{Fl} + 3n$	1880	205.19	245.56	0.67	0.64	0.19	190.22	0.77	1.04	4.0 pb	$3.6^{+3.4}_{-1.7}$ pb [35]	Used
$^{43}_{20}\text{Ca} + ^{240}_{94}\text{Pu} \rightarrow ^{280}_{114}\text{Fl} + 3n$	1880	209.87	247.47	0.70	0.65	0.40	193.46	0.80	1.04	2.81 nb		Prop.
$^{36}_{18}\text{Ar} + ^{246}_{96}\text{Cm} \rightarrow ^{278}_{114}\text{Fl} + 4n$	1728	207.16	237.47	0.74	0.68	0.56	180.61	0.79	1.04	47 pb		Prop.
$^{48}_{20}\text{Ca} + ^{243}_{95}\text{Am} \rightarrow ^{288}_{115}\text{Mc} + 3n$	1900	206	247.69	0.67	0.65	0.15	192.41	0.78	1.04	2.0 pb	$2.7^{+4.8}_{-1.6}$ pb [76]	Used
$^{46}_{21}\text{Sc} + ^{244}_{94}\text{Pu} \rightarrow ^{287}_{115}\text{Mc} + 3n$	1974	215.87	256.56	0.68	0.63	0.41	200.78	0.81	1.04	17.8 nb		Prop.
$^{38}_{18}\text{Ar} + ^{246}_{97}\text{Bk} \rightarrow ^{281}_{115}\text{Mc} + 3n$	1746	199.87	230.74	0.73	0.69	0.42	181.35	0.79	1.04	2.51 nb		Prop.
$^{48}_{21}\text{Sc} + ^{240}_{94}\text{Pu} \rightarrow ^{285}_{115}\text{Mc} + 3n$	1974	223.87	268.64	0.67	0.63	0.27	200.43	0.81	1.04	0.298 μb		Prop.
$^{51}_{23}\text{V} + ^{236}_{92}\text{U} \rightarrow ^{284}_{115}\text{Mc} + 3n$	2116	239.87	291.70	0.64	0.60	0.35	213.99	0.84	1.04	19.5 nb		Prop.
$^{48}_{20}\text{Ca} + ^{248}_{96}\text{Cm} \rightarrow ^{292}_{116}\text{Lv} + 4n$	1920	209.14	249.56	0.67	0.65	0.18	193.60	0.78	1.04	2.67 pb	$3.3^{+2.5}_{-1.4}$ pb [35]	Used
$^{36}_{18}\text{Ar} + ^{249}_{98}\text{Cf} \rightarrow ^{282}_{116}\text{Lv} + 3n$	1764	197.87	226.47	0.75	0.69	0.54	183.88	0.80	1.04	0.195 nb		Prop.
$^{41}_{20}\text{Ca} + ^{240}_{96}\text{Cm} \rightarrow ^{278}_{116}\text{Lv} + 3n$	1920	217.87	255.09	0.71	0.66	0.45	198.70	0.83	1.03	0.129 nb		Prop.
$^{36}_{18}\text{Ar} + ^{252}_{98}\text{Cf} \rightarrow ^{284}_{116}\text{Lv} + 4n$	1764	209.16	239.04	0.75	0.69	0.57	183.40	0.80	1.04	0.289 nb		Prop.
$^{48}_{20}\text{Ca} + ^{249}_{97}\text{Bk} \rightarrow ^{293}_{117}\text{Ts} + 4n$	1940	211.23	251.95	0.67	0.65	0.16	195.45	0.79	1.03	1.78 pb	$0.5^{+1.1}_{-0.4}$ pb [77]	Used
$^{48}_{20}\text{Ca} + ^{249}_{97}\text{Bk} \rightarrow ^{294}_{117}\text{Ts} + 3n$	1940	211.29	252.03	0.67	0.65	0.16	195.45	0.79	1.03	0.37 pb	$1.3^{+1.5}_{-0.6}$ pb [77]	Used
$^{46}_{20}\text{Ca} + ^{243}_{97}\text{Bk} \rightarrow ^{287}_{117}\text{Ts} + 2n$	1940	214.58	255.20	0.68	0.66	0.21	197.49	0.81	1.03	28.2 nb		Prop.
$^{48}_{20}\text{Ca} + ^{248}_{97}\text{Bk} \rightarrow ^{293}_{117}\text{Ts} + 3n$	1940	221.87	264.81	0.68	0.66	0.16	195.62	0.79	1.04	0.956 μb		Prop.
$^{40}_{20}\text{Ca} + ^{249}_{98}\text{Cf} \rightarrow ^{294}_{118}\text{Og} + 3n$	1960	226.08	269.66	0.67	0.66	0.14	197.47	0.79	1.03	2.68 pb	$2.2^{+2.6}_{-0.8}$ pb [78]	Used
$^{52}_{24}\text{Cr} + ^{244}_{94}\text{Pu} \rightarrow ^{293}_{118}\text{Og} + 3n$	2256	249.87	303.12	0.65	0.59	0.43	226.02	0.87	1.03	33.1 nb		Prop.
$^{47}_{20}\text{Ca} + ^{252}_{98}\text{Cf} \rightarrow ^{296}_{118}\text{Og} + 3n$	1960	222.87	264.43	0.69	0.66	0.22	197.48	0.80	1.03	0.223 μb		Prop.
$^{40}_{20}\text{Ca} + ^{253}_{98}\text{Cf} \rightarrow ^{288}_{118}\text{Og} + 5n$	1960	240.45	278.46	0.73	0.66	0.58	201.14	0.84	1.03	0.512 nb		Prop.
$^{50}_{23}\text{V} + ^{250}_{96}\text{Cm} \rightarrow ^{297}_{119} + 3n$	2208	239.87	287.84	0.67	0.61	0.43	221.16	0.86	1.03	84.2 nb		Prop.
$^{53}_{25}\text{Mn} + ^{239}_{94}\text{Pu} \rightarrow ^{289}_{119} + 3n$	2350	262.87	321.16	0.64	0.58	0.42	235.89	0.89	1.03	20.4 nb		Prop.
$^{44}_{22}\text{Ti} + ^{249}_{98}\text{Cf} \rightarrow ^{292}_{120} + 1n$	2156	238.16	289.68	0.69	0.63	0.26	219.51	0.87	1.02	19.18 pb		Prop.
$^{47}_{22}\text{Ti} + ^{249}_{98}\text{Cf} \rightarrow ^{295}_{120} + 1n$	2156	244.38	290.51	0.68	0.63	0.40	217.77	0.85	1.02	18.55 pb		Prop.
$^{50}_{22}\text{Ti} + ^{249}_{98}\text{Cf} \rightarrow ^{298}_{120} + 1n$	2156	242.59	291.32	0.66	0.63	0.26	216.13	0.84	1.02	14.88 pb		Prop.
$^{64}_{28}\text{Ni} + ^{239}_{93}\text{Np} \rightarrow ^{301}_{121} + 2n$	2604	277.58	351.91	0.58	0.54	0.28	255.15	0.91	1.02	0.275 μb		Prop.
$^{48}_{23}\text{V} + ^{252}_{98}\text{Cf} \rightarrow ^{297}_{121} + 3n$	2254	244.87	291.51	0.68	0.62	0.48	226.52	0.88	1.02	1.32 nb		Prop.
$^{49}_{23}\text{V} + ^{253}_{98}\text{Cf} \rightarrow ^{299}_{121} + 3n$	2254	245.87	293.49	0.68	0.62	0.45	225.76	0.87	1.02	5.04 nb		Prop.

TABLE II. (*Continued.*)

Reaction	Z_1Z_2	E_{cm}	E_{lab}	η	α_z	$\Delta(N/Z)$	z	χ_m	α_{BG}	σ_{ER}^{Theo}	σ_{ER}^{Expt}	Remark
$^{85}_{36}\text{Kr} + ^{225}_{86}\text{Rn} \rightarrow ^{310}_{122} + 0n$	3086	320.00	440.89	0.45	0.41	0.26	295.45	0.97	1.02	10 nb		Prop.
$^{86}_{37}\text{Rb} + ^{223}_{85}\text{At} \rightarrow ^{308}_{122} + 1n$	3145	333.29	461.82	0.44	0.39	0.30	300.15	0.97	1.02	0.23 nb		Prop.
$^{76}_{32}\text{Ge} + ^{239}_{91}\text{Pa} \rightarrow ^{314}_{123} + 1n$	2912	296.29	390.51	0.52	0.48	0.25	278.88	0.94	1.02	0.128 nb		Prop.
$^{72}_{30}\text{Zn} + ^{242}_{93}\text{Np} \rightarrow ^{313}_{123} + 1n$	2790	287.29	372.76	0.54	0.51	0.20	268.48	0.92	1.02	0.36 nb		Prop.
$^{64}_{30}\text{Zn} + ^{240}_{93}\text{Np} \rightarrow ^{302}_{123} + 2n$	2790	294.58	373.13	0.58	0.51	0.45	273.14	0.95	1.01	2.01 nb		Prop.
$^{71}_{33}\text{As} + ^{232}_{90}\text{Th} \rightarrow ^{301}_{123} + 2n$	2970	314.58	410.85	0.53	0.46	0.43	288.76	0.98	1.01	1.15 nb		Prop.
$^{72}_{30}\text{Zn} + ^{244}_{94}\text{Pu} \rightarrow ^{315}_{124} + 1n$	2820	292.29	378.54	0.54	0.52	0.20	270.92	0.93	1.02	0.5 nb		Prop.
$^{72}_{30}\text{Zn} + ^{242}_{94}\text{Pu} \rightarrow ^{313}_{124} + 1n$	2820	294.29	381.85	0.54	0.52	0.17	271.37	0.93	1.02	0.876 nb		Prop.
$^{85}_{36}\text{Kr} + ^{227}_{89}\text{Ac} \rightarrow ^{311}_{125} + 1n$	3204	331.29	454.80	0.46	0.42	0.23	301.54	0.98	1.01	11.8 nb		Prop.
$^{58}_{28}\text{Ni} + ^{245}_{97}\text{Bk} \rightarrow ^{302}_{125} + 1n$	2716	287.29	355.30	0.62	0.55	0.45	268.16	0.96	1.01	0.631 nb		Prop.
$^{66}_{28}\text{Ni} + ^{249}_{97}\text{Bk} \rightarrow ^{314}_{125} + 1n$	2716	284.29	359.64	0.58	0.55	0.21	262.86	0.92	1.01	0.416 nb		Prop.
$^{60}_{28}\text{Ni} + ^{247}_{97}\text{Bk} \rightarrow ^{305}_{125} + 1n$	2716	294.58	366.14	0.61	0.55	0.40	266.56	0.95	1.01	19.3 nb		Prop.
$^{83}_{36}\text{Kr} + ^{232}_{90}\text{Th} \rightarrow ^{315}_{126} + 0n$	3240	339	460.28	0.47	0.43	0.27	308.37	0.99	1.00	0.352 nb		Prop.
$^{82}_{36}\text{Kr} + ^{232}_{90}\text{Th} \rightarrow ^{314}_{126} + 0n$	3240	339	458.82	0.48	0.43	0.30	308.89	1.0	1.00	31 nb		Prop.

as a function of z as follows:

$$\sigma_{ER} = 10^{-0.04248z+7.75395}. \quad (40)$$

Thus, it is obvious from the three equations just given above that z plays an important role in the synthesis of the superheavy elements. We can gauge from Fig. 5 that Eq. (39) may give quite a correct estimation of the fusion barrier. However, the scenario is not the same for P_{CN} and σ_{ER} as apparent from Figs. 4 and 6. For a fixed z , the values of P_{CN} and σ_{ER} vary up to about 3 orders and thus do not have much use. One needs to follow the theoretical calculations given above. It is clear from Eqs. (38) and (40) that P_{CN} and σ_{ER} decrease with increases of z . However, this statement is not sacrosanct as it can obviously be realized from Table II. A lot of departure can be visualized there; for example, the reactions $^{46}_{20}\text{Ca} + ^{243}_{97}\text{Bk}$ with $z = 197.49$ and $^{82}_{36}\text{Kr} + ^{232}_{90}\text{Th}$ with $z = 308.89$ lead to similar $\sigma_{ER} = 28.2$ and 31.0 nb, respectively. Furthermore,

the reactions $^{83}_{36}\text{Kr} + ^{232}_{90}\text{Th}$ and $^{82}_{36}\text{Kr} + ^{232}_{90}\text{Th}$ have nearly equal $z \approx 308$, but have about 2 orders of magnitude different σ_{ER} , 0.35 and 31 nb, respectively. These imply that the heavy ion reactions are very complex; the occurrence of a certain phenomenon depends on several entrance channel parameters and other postcollision properties. Thus, the values of P_{CN} and σ_{ER} are governed not only by z but also by other entrance channel parameters like mass asymmetry (η), charge asymmetry (α_z), isospin asymmetry [$\Delta(N/Z)$], mean fissility χ_m , and Businaro-Gallone mass asymmetry (α_{BG}), as discussed here, and the projectile energy and deformation parameter, etc., which will be examined in forthcoming works.

5. Non-compound nucleus fission (NCNF)

According to the model proposed by Ramamurthy and Kapoor [26], the probability of non-compound nuclear fission

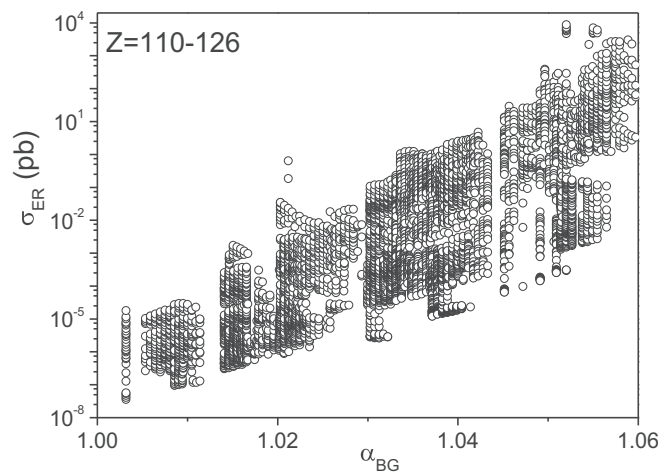


FIG. 2. Variation of the evaporation residue cross sections with the Businaro-Gallone mass asymmetry for the superheavy nuclei with $Z = 110-126$.

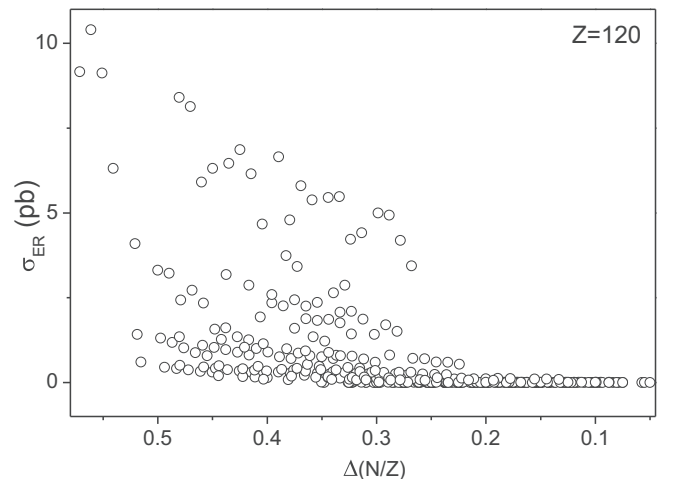


FIG. 3. Variation of the evaporation residue cross sections as a function of isospin asymmetry for the superheavy nuclei with $Z = 120$.

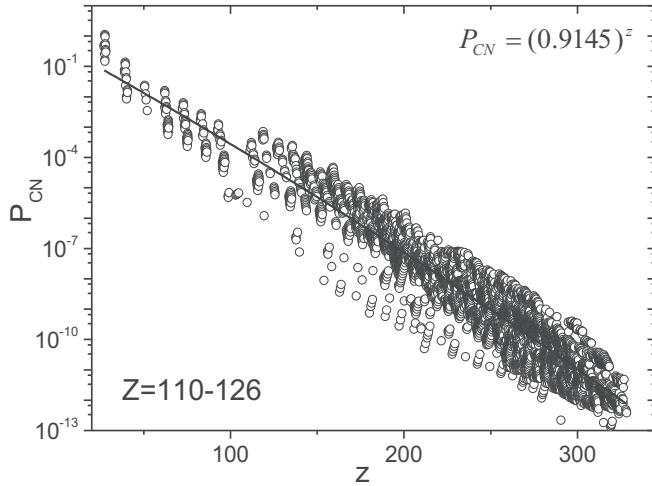


FIG. 4. Variation of the compound nucleus formation probability with the Coulomb interaction parameter z for the superheavy elements with $Z = 110-126$.

(P_{NCNF}) is expressed as

$$P_{\text{NCNF}} = \exp\left[\frac{-0.5B_f}{T_{\text{sad}}}\right], \quad (41)$$

where B_f is the fission barrier and T_{sad} is the temperature of the saddle point. We have studied the contributions of NCNF in induced fission of the superheavy nuclei with $110 < Z < 126$ for the different projectile-target combinations. Figure 7 shows the contribution of non-compound nucleus fission in the evaporation residue cross sections in the case of $3n$ for the superheavy nuclei with $Z = 120$. From the figure it is observed that as the P_{NCNF} increases the corresponding evaporation residue cross section decreases.

6. Hindrance of quasifission

The study of fusion dynamics in the vicinity of the Coulomb barrier energies shows that the complete fusion of

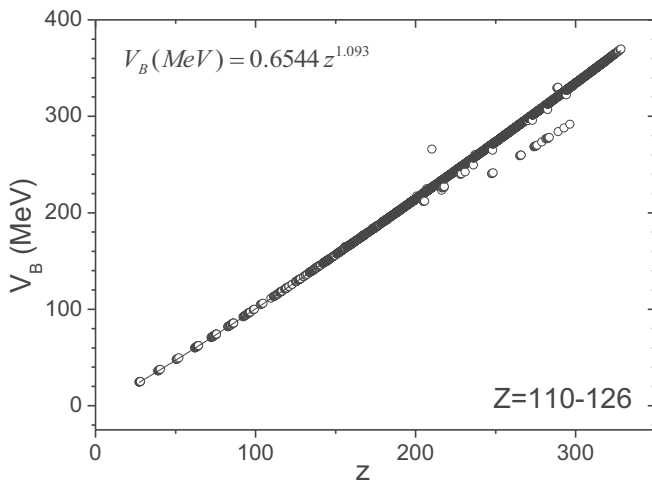


FIG. 5. Variation of the fusion barrier with the Coulomb interaction parameter z for the superheavy elements with $Z = 110-126$.

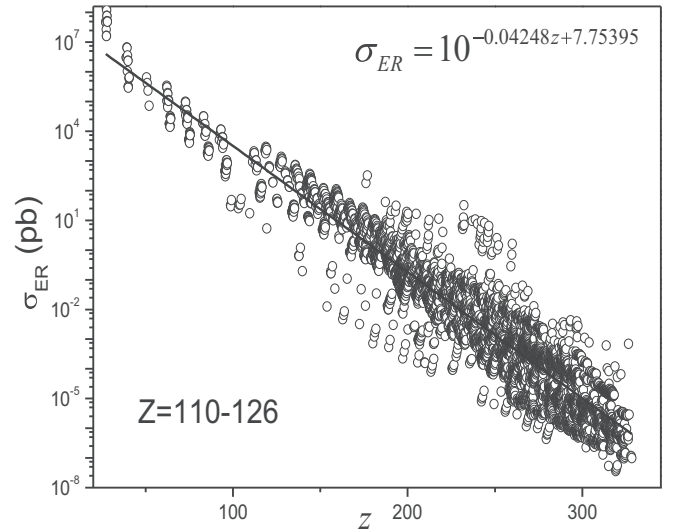


FIG. 6. Variation of the evaporation residue cross section with the Coulomb interaction parameter z for the superheavy elements with $Z = 110-126$.

reactants does not occur immediately upon nuclei contact. During the heavy ion reactions, the whole process of fusion is severely hampered by deep inelastic, quasifission, and fast fission processes, and among these processes the formation of compound nuclei is primarily hindered by quasifission. The quasifission process occurs with the multinucleon or cluster transfer and the dinuclear system begins to break down into two fragments without attaining the compound nucleus formation. Because there is a competition between the compound nucleus formation and quasifission, knowing the quasifission probability helps us to analyze the probability of the compound nucleus formation in the synthesis of superheavy nuclei.

To choose a good projectile-target combination for the synthesis of superheavy nuclei, we have studied the parameters,

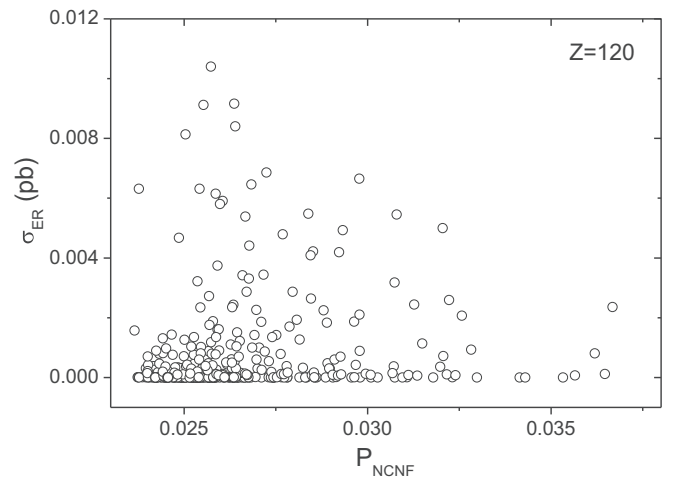


FIG. 7. Variation of the evaporation residue cross sections for the $3n$ channel versus the non-compound nuclear fusion probability for the superheavy nuclei with $Z = 120$.

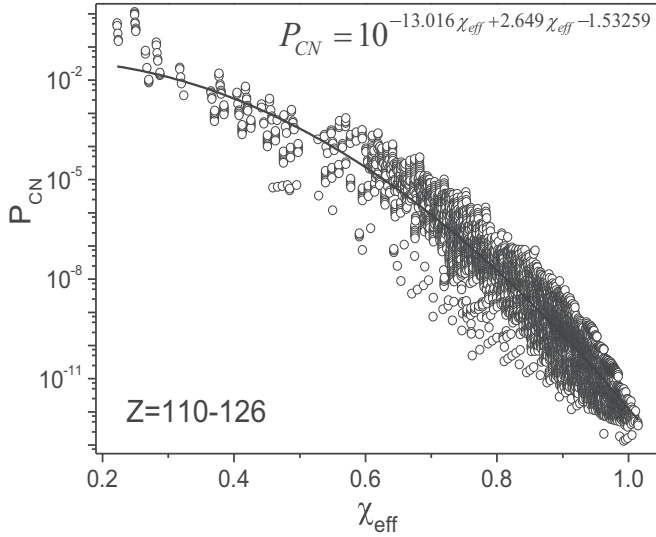


FIG. 8. Variation of the compound nucleus formation probability of the superheavy nuclei with $Z = 110-126$ with the effective entrance channel fissility.

such as the compound nucleus fissility χ_{eff} , the critical ratio Z^2/A , the mean fissility χ_m , and the critical value α_{CR} , that are related to the quasifission probability. The compound nucleus fissility χ_{CN} reflects the stability of the compound nuclei against the fission as

$$\chi_{\text{CN}} = \frac{Z^2/A}{\chi} = \frac{Z^2/A}{50.883[1 - 1.7826(\frac{A-2Z}{A})^2]}. \quad (42)$$

The effective entrance channel fissility (χ_{eff}) corresponding to the repulsive and attractive forces was estimated as follows:

$$\chi_{\text{eff}} = \frac{4Z_1Z_2}{(A_1^{1/3} + A_2^{1/3}) \times (A_1A_2)^{1/3}} \cdot \frac{1}{50.883[1 - 1.7826(\frac{A-2Z}{A})^2]}. \quad (43)$$

The mean fissility χ_m often indicates the appearance of the quasifission and it is expressed as

$$\chi_m = 0.25\chi_{\text{CN}} + 0.75\chi_{\text{eff}} \quad (44)$$

Here the quasifission becomes dominant when $\chi_m > 0.765$ [73,81]. The feasibility of the quasifission depends on the mass asymmetry (η) of the entrance channel and the quasifission process occurs only when the mass asymmetry is smaller than the critical value as follows:

$$\alpha_{\text{CR}} = \begin{cases} 0 & \text{if } \chi_{\text{CN}} < 0.396, \\ 1.12\sqrt{\frac{\chi_{\text{CN}} - 0.396}{\chi_{\text{CN}} - 0.156}} & \text{if } \chi_{\text{CN}} > 0.396. \end{cases} \quad (45)$$

We have studied the variation of the compound nucleus probability and the evaporation residue cross sections with the effective entrance-channel fissility χ_{eff} . Figures 8 and 9 show the variation of the compound nucleus probability and the evaporation residue cross sections with the effective entrance channel fissility χ_{eff} . From both figures it is observed that as the χ_{eff} increases the corresponding compound nucleus probability and evaporation residue cross sections decrease. Hence, to get the maximum cross sections during the fusion

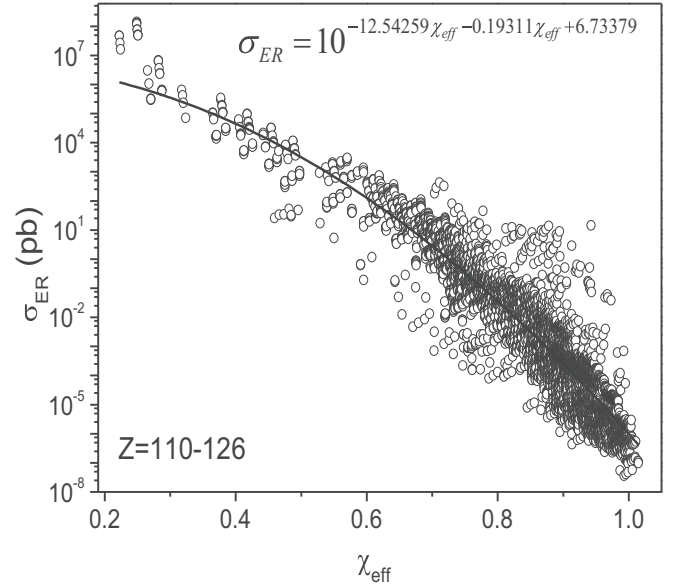


FIG. 9. Variation of the evaporation residue cross sections of the superheavy nuclei with $Z = 110-126$ with the effective entrance channel fissility.

of a certain projectile and target combination, the χ_{eff} must be kept to a minimum. We have exercised regressions to find the best equations for the compound nucleus formation probability and evaporation residue cross sections as a function of the χ_{eff} ; they are as follows:

$$P_{\text{CN}} = 10^{-13.016\chi_{\text{eff}}^2 + 2.694\chi_{\text{eff}} - 1.53259} \quad (46)$$

and

$$\sigma_{\text{ER}} = 10^{-12.54259\chi_{\text{eff}}^2 - 0.19311\chi_{\text{eff}} + 6.73379}. \quad (47)$$

The hindrance of the quasifission dominates the formation of compound nuclei due to its high fissility. Figure 10 shows the variation of the mean fissility χ_m as a function of Z_1Z_2 . From the figure it is observed that the mean fissility χ_m increases

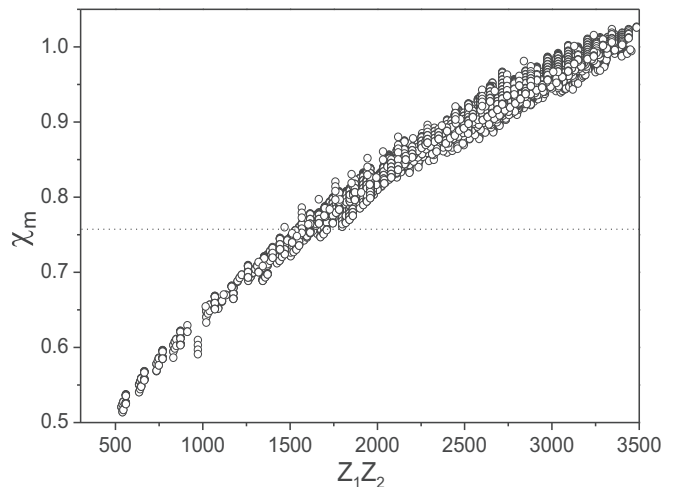
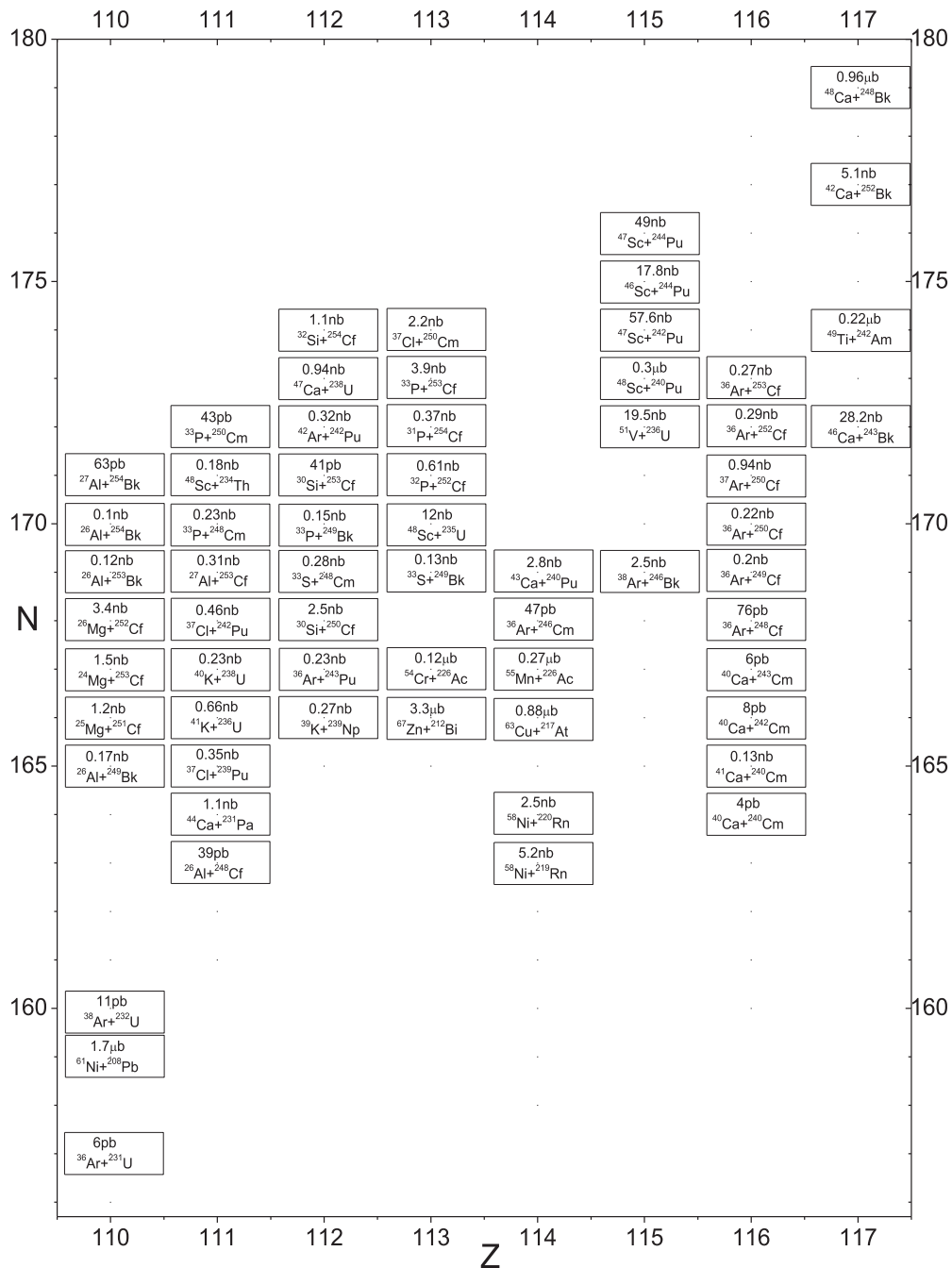


FIG. 10. Variation of χ_m as a function of Z_1Z_2 for the synthesis of the superheavy elements $Z = 100-126$.


 FIG. 11. Chart of suitable projectile-target combinations to synthesize the superheavy elements with $Z = 110-117$.

as the corresponding value of Z_1Z_2 also increases. Furthermore, when the mean fissility $\chi > 0.765$, the quasifission is dominant, and for $\chi < 0.765$ the probability of the compound nucleus formation dominates over the quasifission.

Figure 11 represents a chart of suitable projectile-target combinations to synthesize the superheavy elements with $Z = 110-117$, and Fig. 12 displays the same for the elements with $Z = 118-126$ with respect to the corresponding production cross section. By the study of the entrance channel effects on the evaporation residue cross sections, it can be clearly seen why the reaction $^{25}\text{Mg} + ^{251}\text{Cf} \rightarrow ^{272}_{110}\text{Ds} + 4n$ leads to the maximum evaporation residue cross section of

1.19 nb when compared to all other projectile-target combinations. A similar situation is seen with other proposed reactions for the synthesis of the superheavy elements with $Z = 111-126$. Accordingly we have predicted the most possible projectile-target combinations for the superheavy nuclei with $Z = 110-117$ along with the evaporation residue cross sections; they are shown in Fig. 11. Hence, we have successfully represented all the projectile-target combinations and their evaporation residue cross sections in a single chart. Correspondingly, the best possible projectile-target combinations to synthesize the superheavy elements with $Z = 118-126$ are shown in Fig. 12.

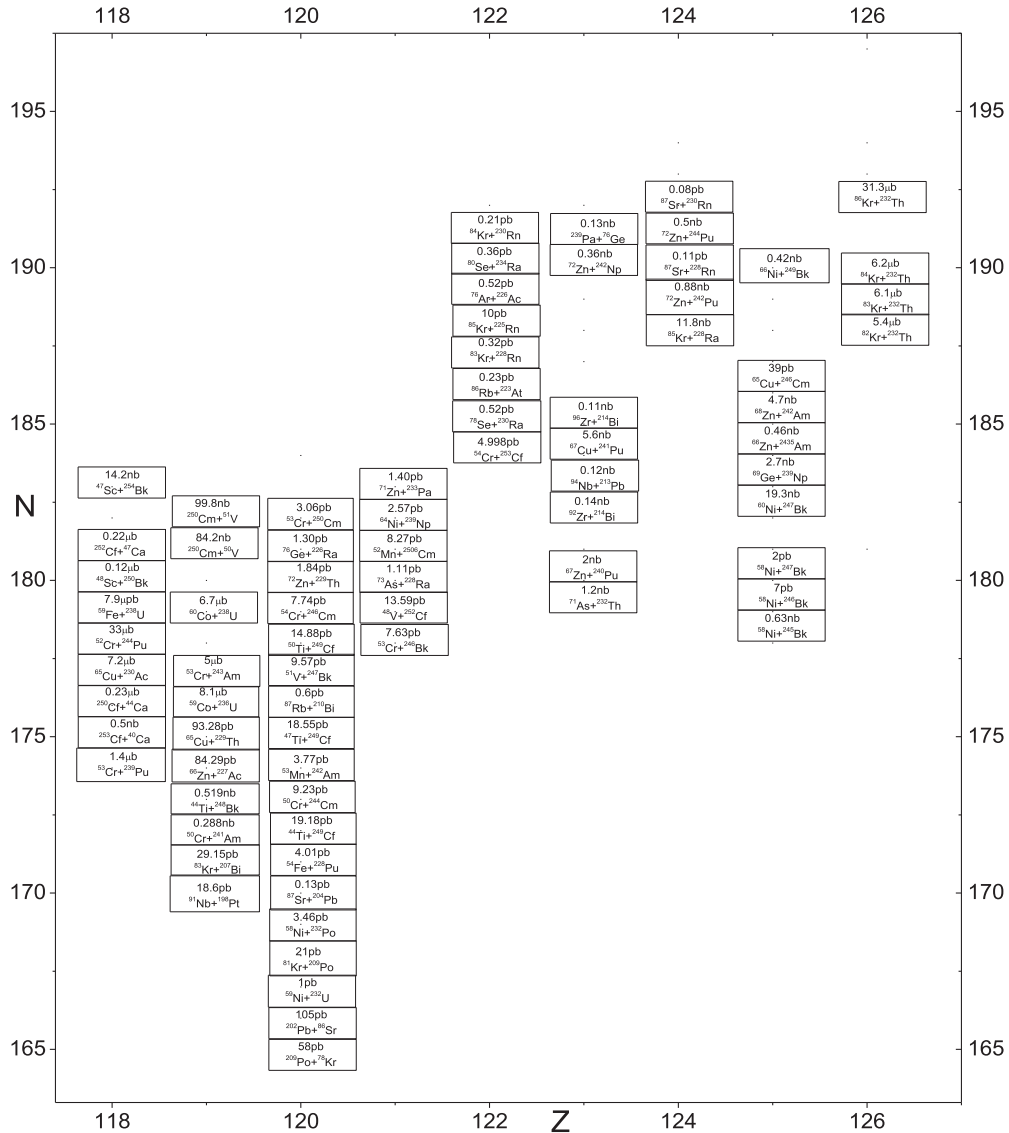


FIG. 12. Chart of suitable projectile-target combinations to synthesize the superheavy elements with $Z = 118$ – 126 .

The existence of the superheavy nuclei depends on the interaction between the short-range attractive nuclear force and the long-range electrostatic repulsion. The latter becomes stronger at the larger values of Z_1Z_2 . Table I gives the ranges of the possible projectile-target combinations. Furthermore, Table II lists the entrance channel effects such as mass asymmetry (η), charge asymmetry (α_Z), isospin asymmetry ($\Delta \frac{N}{Z}$), Coulomb charge (Z_1Z_2), mean fissility (χ_m), Businaro-Gallone mass asymmetry (α_{BG}), and corresponding evaporation residue cross sections for the synthesis of superheavy nuclei with $Z = 110$ – 126 . Note that the beam energy quoted in Table II is one for which the σ_{ER} is found to be maximum. However, the reactions already utilized in past experiments are the same as those given in Table II. From the analysis of Table II, the entrance channel effects such as mass and charge asymmetry will have smaller values (mind the negative sign of η) with the maximum evaporation cross sections as discussed in the Fig. 1. Similarly the larger the value of the isospin asymmetry is, the higher the correspond-

ing σ_{ER} is. When the Coulomb charge asymmetry values are smaller, then the corresponding values of σ_{ER} are found to be higher. In addition to the entrance channel effects such as charge asymmetry, mass asymmetry, and isospin asymmetry, we have also studied the hindrance of the quasifission in the predicted projectile-target combinations. Here the quasifission dominates over the fusion of the two nuclei at $\chi > 0.765$. Even though the quasifission dominates the complete fusion process, but the σ_{ER} depends on the other parameters such as the charge, mass, isospin, Coulomb charge asymmetry and the probability of NCNF which dominates over the quasifission. The contribution of NCNF for the fusion systems exhibits its role when the value of the mass asymmetry η is greater than the Businaro-Gallone mass asymmetry α_{BG} . However, there is no fusion suppression due to the quasifission on the evaporation residue cross sections for the less asymmetric systems.

The prediction of the theoretical model is successful when the results produced are in agreement with the experimental

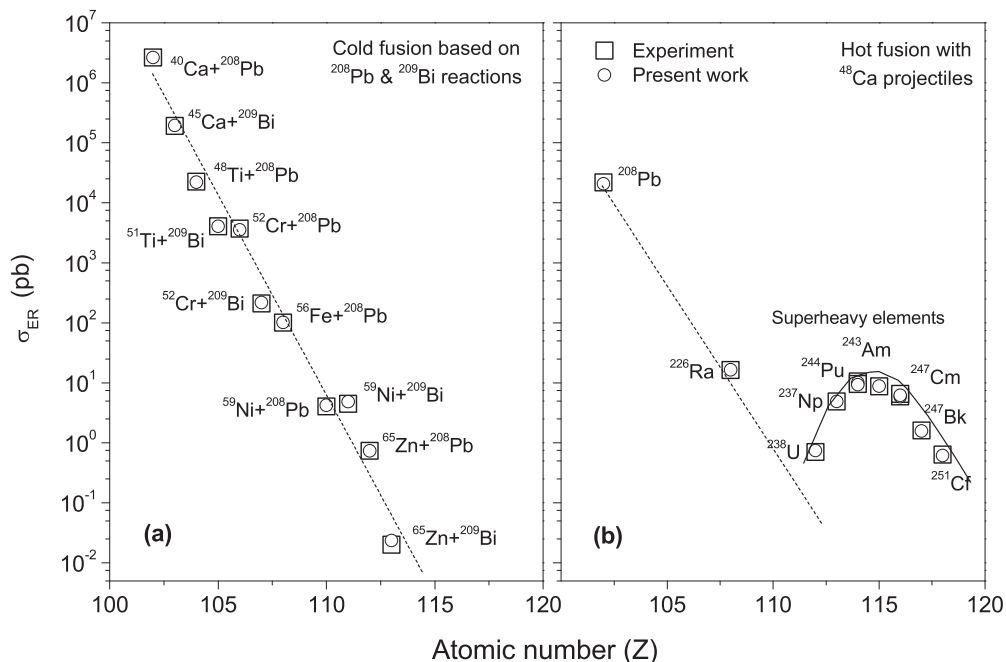


FIG. 13. Experimental (open squares) and theoretical (open circles) evaporation residue cross sections for the synthesis of the elements with $Z = 102$ – 113 from the cold fusion reactions (a) and the elements with $Z = 112$ – 118 from the hot fusion reactions (b). In the cold fusion reactions both the projectiles and the targets are shown against every data point, whereas only the target is labeled for the hot fusion reactions as the projectile remained fixed as ^{48}Ca .

values [82]. Figures 13(a) and 13(b) show the production cross sections for both the cold fusion reactions by using lead and bismuth as targets and the hot fusion reactions by using calcium as the projectile. The significant result of the cold fusion experiment shows relatively high probability of the evaporation residue cross sections for the lower value of the compound nuclear atomic number, $Z \leq 110$, and gradually the production cross section decreases with the increase in the atomic number. In contrast, the hot fusion reactions exhibit low cross sections for $Z \leq 113$, gradually increase to a certain maximum for $Z = 115$, and then again decrease to a sub-picobarn for $Z = 118$. The comparison of present predictions have included experiments for both the cold and hot fusion reactions. It is noteworthy that the agreement between present predictions and experimental values is very good for the hot fusion reactions, whereas the agreement is not so good for two cold fusion reactions; a factor of 3 difference and an order of magnitude difference between the predictions and the experimental values are seen for $^{272}_{111}\text{Rg}$ and $^{278}_{113}\text{Nh}$, respectively. Because the hot fusion can only be utilized for synthesizing the new elements with $Z > 118$, the present predictions provide evidence for the reliability of the experiments targeting to produce the superheavy elements with $Z > 118$.

B. Decay properties

If a superheavy nucleus is stable against spontaneous fission, then it will decay through other decay modes such as α decay and β decay. The probabilities of these decay modes have been determined by the study of their lifetimes. The latter can be calculated by using the models explained in

previous works [39–46]. The estimation of lifetimes is based on the study of the Coulomb potential and nuclear interaction between two nuclei. Figure 14 shows the decay chain of the nuclei $^{283}_{112}\text{Cn}$; it undergoes 1α decay with the half-lives of 20 ns and similarly we have observed the consistent α -decay chain up to ^{251}Cm with the gradual increase in the half-lives as it reaches near the stable nuclei. In the case of ^{255}Cf it decays to ^{251}Cm with α -decay half-lives of 19 s. Finally ^{251}Cm terminates at ^{251}Bk with the β decay, and the consistent decay chains of ^{251}Bk are shown in Fig. 14. Similarly, we have studied the decay chains for other superheavy nuclei with $Z = 114$ – 118 and also predicted sequential decay chains of the

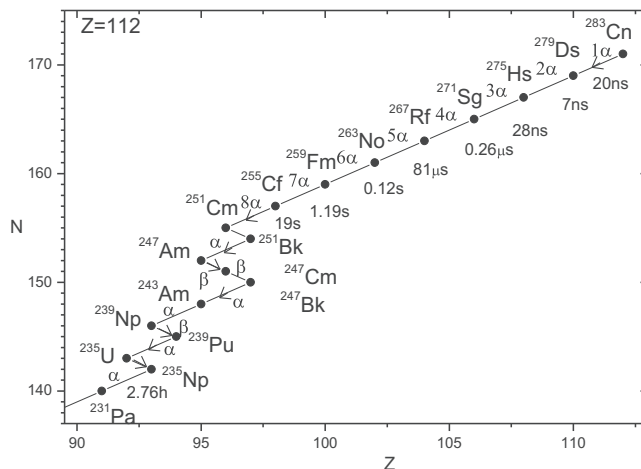


FIG. 14. Decay series of $^{283}_{112}\text{Cn}$.

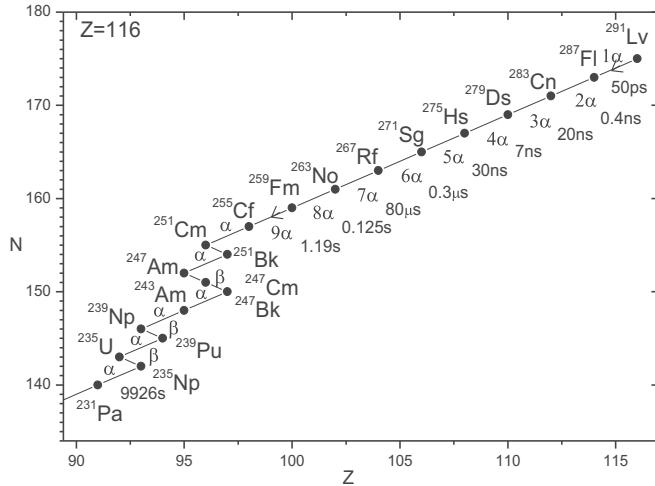


FIG. 15. Decay series of $^{291}_{116}\text{Lv}$.

nuclei with $Z = 119$ and 120 . We have shown the decay of superheavy nuclei with atomic number Z as follows: $Z = 116$ in Fig. 15, $Z = 118$ in Fig. 16, $Z = 119$ in Fig. 17, and $Z = 120$ in Fig. 18. The predicted decay chains are useful in the synthesis of the superheavy elements.

IV. SUMMARY

We have studied many possible projectile-target combinations to synthesize the superheavy nuclei with atomic number $110 \leq Z \leq 126$. The entrance channel effects such as mass asymmetry, charge asymmetry, isospin asymmetry, non-compound nucleus fission probability, Businaro-Gallone mass asymmetry, and hindrance of quasifission have been investigated in search of good projectile-target combinations to synthesize the superheavy elements. Our predictions on the evaporation residue cross section compare very well with the superheavy compound nuclei with atomic number $110 \leq Z \leq 118$. With this confidence level, we have constructed two charts that depict the preferred projectile-target combi-

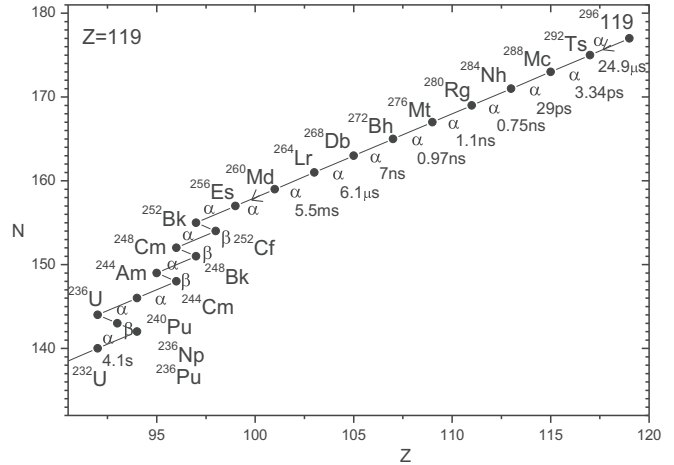


FIG. 17. Decay series of $^{296}_{119}$.

nations for synthesizing the superheavy nuclei with atomic number $110 \leq Z \leq 126$. The present work will certainly be a road map for the synthesis of the superheavy elements with $Z > 118$. Very interestingly, the past reactions used for the realization of the superheavy elements in the laboratory have led to evaporation residue cross sections < 5 pb. In contrast, this work suggests many reactions that lead to hundreds of picobarns to close to a microbarn evaporation residue cross section. Of course, some projectiles or targets are not naturally abundant, and such difficulties were prevalent with the used reactions too. Very strikingly, there are proposed reactions containing both projectiles and targets that are naturally abundant, e.g., $^{82}_{36}\text{Kr} + ^{232}_{90}\text{Th} \rightarrow ^{314}_{126} + 0n$. This reaction leads to the superheavy nuclei with $Z = 126$ with evaporation residue cross sections as high as 31 nb. This cross section is as large as the one obtained for the production of the first superheavy element with $Z = 104$ using the reaction $^{48}_{22}\text{Ti} + ^{208}_{82}\text{Pb}$. Hence, the presently available experimental scenario is up to the right mark. Even the exposure of a beam for a week will test the prediction and finally make a dream come true by entering the eighth row of the periodic table.

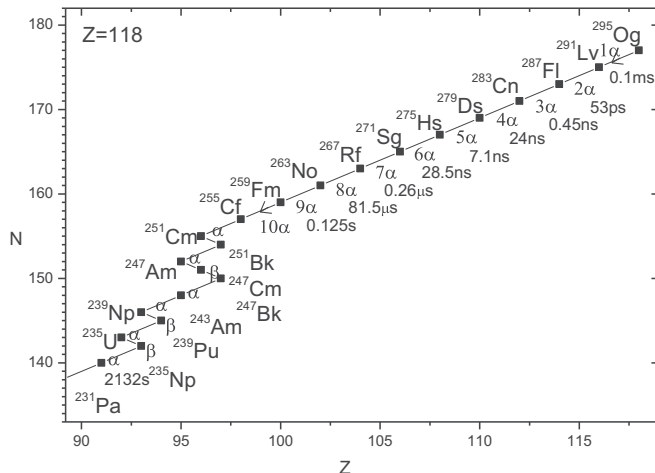


FIG. 16. Decay series of $^{295}_{118}\text{Og}$.

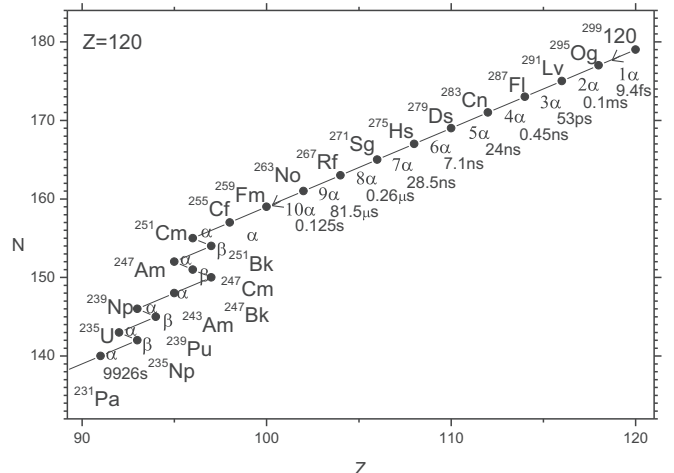


FIG. 18. Decay series of $^{299}_{120}$.

- [1] S. Hofmann and G. Münzenberg, *Rev. Mod. Phys.* **72**, 733 (2000).
- [2] K. Morita, K. Morimoto, D. Kaji, T. Akiyama, S.-i. Goto, H. Haba, E. Ideguchi, K. Katori, H. Koura, H. Kudo *et al.*, *J. Phys. Soc. Jpn.* **76**, 043201 (2007).
- [3] Yu. Ts. Oganessian, V. K. Utyonkov, Y. V. Lobanov, F. S. Abdullin, A. N. Polyakov, R. N. Sagaidak, I. V. Shirokovsky, Y. S. Tsyganov, A. A. Voinov, G. G. Gulbekian, S. L. Bogomolov, B. N. Gikal, A. N. Mezentsev, S. Iliev, V. G. Subbotin, A. M. Sukhov, K. Subotic, V. I. Zagrebaev, G. K. Vostokin, M. G. Itkis *et al.* *Phys. Rev. C* **74**, 044602 (2006).
- [4] S. Hofmann, D. Ackermann, S. Antalic, H. Burkhard, V. Comas, R. Dressler, Z. Gan, S. Heinz, J. Heredia, F. Heßberger *et al.*, *Eur. Phys. J. A* **32**, 251 (2007).
- [5] S. Hofmann, V. Ninov, F. Heßberger, P. Armbruster, H. Folger, G. Münzenberg, H. Schött, A. Popeko, A. Yerein, A. Andreyev *et al.*, *Z. Phys. A: Hadrons Nucl.* **350**, 277 (1995).
- [6] P. Armbruster, *Annu. Rev. Nucl. Part. Sci.* **35**, 135 (1985).
- [7] G. Münzenberg, *Rep. Prog. Phys.* **51**, 57 (1988).
- [8] W. Swiatecki, *Prog. Part. Nucl. Phys.* **4**, 383 (1979).
- [9] S. Bjørnholm and W. J. Swiatecki, *Nucl. Phys. A* **391**, 471 (1982).
- [10] Y. Aritomo, T. Wada, M. Ohta, and Y. Abe, *Phys. Rev. C* **59**, 796 (1999).
- [11] V. I. Zagrebaev, *Phys. Rev. C* **64**, 034606 (2001).
- [12] V. Zagrebaev, Y. Aritomo, M. G. Itkis, Yu. Ts. Oganessian, and M. Ohta, *Phys. Rev. C* **65**, 014607 (2001).
- [13] E. Chabanat, P. Bonche, P. Haensel, J. Meyer, and R. Schaeffer, *Nucl. Phys. A* **627**, 710 (1997).
- [14] G. Adamian, N. Antonenko, W. Scheid, and V. Volkov, *Nucl. Phys. A* **633**, 409 (1998).
- [15] Z.-Q. Feng, G.-M. Jin, F. Fu, and J.-Q. Li, *Nucl. Phys. A* **771**, 50 (2006).
- [16] N. Wang, Z. Li, X. Wu, J. Tian, Y. X. Zhang, and M. Liu, *Phys. Rev. C* **69**, 034608 (2004).
- [17] A. Kataev, *Mod. Phys. Lett. A* **20**, 2007 (2005).
- [18] Z.-Q. Feng, G.-M. Jin, and F.-S. Zhang, *Nucl. Phys. A* **802**, 91 (2008).
- [19] Z.-Q. Feng, F.-S. Zhang, G.-M. Jin, and X. Huang, *Nucl. Phys. A* **750**, 232 (2005).
- [20] F. Zhao-Qing, J. Gen-Ming, Z. Feng-Shou, F. Fen, and H. Xi, *Chin. Phys. Lett.* **22**, 3040 (2005).
- [21] R. Bock, Y. Chu, M. Dakowski, A. Gobbi, E. Grosse, A. Olmi, H. Sann, D. Schwalm, U. Lynen, W. Müller *et al.*, *Nucl. Phys. A* **388**, 334 (1982).
- [22] J. Töke, R. Bock, G. Dai, A. Gobbi, S. Gralla, K. Hildenbrand, J. Kuzminski, W. Müller, A. Olmi, H. Stelzer *et al.*, *Nucl. Phys. A* **440**, 327 (1985).
- [23] W. Q. Shen, J. Albinski, A. Gobbi, S. Gralla, K. D. Hildenbrand, N. Herrmann, J. Kuzminski, W. F. J. Müller, H. Stelzer, J. Toke, B. B. Back, S. Bjornholm, and S. P. Sorensen, *Phys. Rev. C* **36**, 115 (1987).
- [24] R. du Rietz, D. J. Hinde, M. Dasgupta, R. G. Thomas, L. R. Gasques, M. Evers, N. Lobanov, and A. Wakhle, *Phys. Rev. Lett.* **106**, 052701 (2011).
- [25] K. T. Lesko, S. Gil, A. Lazzarini, V. Metag, A. G. Seamster, and R. Vandenbosch, *Phys. Rev. C* **27**, 2999 (1983).
- [26] V. S. Ramamurthy and S. S. Kapoor, *Phys. Rev. Lett.* **54**, 178 (1985).
- [27] P. Jisha, A. M. Vinodkumar, B. R. S. Babu, S. Nath, N. Madhavan, J. Gehlot, A. Jhingan, T. Banerjee, I. Mukul, R. Dubey, N. Saneesh, K. M. Varier, E. Prasad, A. Shamlath, P. V. Laveen, and M. Shareef, *Phys. Rev. C* **101**, 024611 (2020).
- [28] G. Mandaglio, A. Anastasi, F. Curciarello, G. Fazio, G. Giardina, and A. K. Nasirov, *Phys. Rev. C* **98**, 044616 (2018).
- [29] S. Soheylly and M. K. Khalili, *Phys. Rev. C* **85**, 034610 (2012).
- [30] T. Nhan Hao, N. Duy, K. Chae, N. Quang Hung, and N. Nhu Le, *Int. J. Mod. Phys. E* **28**, 1950056 (2019).
- [31] G. Giardina, S. Hofmann, A. Muminov, and A. Nasirov, *Eur. Phys. J. A* **8**, 205 (2000).
- [32] D. Hinde and M. Dasgupta, *Phys. Lett. B* **622**, 23 (2005).
- [33] Z. Liu, H. Zhang, J. Xu, Y. Qiao, X. Qian, and C. Lin, *Phys. Lett. B* **353**, 173 (1995).
- [34] D. J. Hinde, M. Dasgupta, J. R. Leigh, J. C. Mein, C. R. Morton, J. O. Newton, and H. Timmers, *Phys. Rev. C* **53**, 1290 (1996).
- [35] Y. T. Oganessian, V. K. Utyonkov, Y. V. Lobanov, F. S. Abdullin, A. N. Polyakov, I. V. Shirokovsky, Y. S. Tsyganov, G. G. Gulbekian, S. L. Bogomolov, B. N. Gikal, A. N. Mezentsev, S. Iliev, V. G. Subbotin, A. M. Sukhov, A. A. Voinov, G. V. Buklanov, K. Subotic, V. I. Zagrebaev, M. G. Itkis, J. B. Patin *et al.*, *Phys. Rev. C* **70**, 064609 (2004).
- [36] G. N. Knyazheva, E. M. Kozulin, R. N. Sagaidak, A. Y. Chizhov, M. G. Itkis, N. A. Kondratiev, V. M. Voskressensky, A. M. Stefanini, B. R. Behera, L. Corradi, E. Fioretto, A. Gadea, A. Latina, S. Szilner, M. Trotta, S. Beghini, G. Montagnoli, F. Scarlassara, F. Haas *et al.*, *Phys. Rev. C* **75**, 064602 (2007).
- [37] D. J. Hinde, R. G. Thomas, R. du Rietz, A. Diaz-Torres, M. Dasgupta, M. L. Brown, M. Evers, L. R. Gasques, R. Rafiei, and M. D. Rodriguez, *Phys. Rev. Lett.* **100**, 202701 (2008).
- [38] K. Nishio, H. Ikezoe, S. Mitsuoka, I. Nishinaka, Y. Nagame, Y. Watanabe, T. Ohtsuki, K. Hirose, and S. Hofmann, *Phys. Rev. C* **77**, 064607 (2008).
- [39] H. C. Manjunatha, *Nucl. Phys. A* **945**, 42 (2016).
- [40] H. C. Manjunatha and N. Sowmya, *Nucl. Phys. A* **969**, 68 (2018).
- [41] H. C. Manjunatha, K. N. Sridhar, and N. Sowmya, *Nucl. Phys. A* **987**, 382 (2019).
- [42] H. C. Manjunatha and K. N. Sridhar, *Nucl. Phys. A* **962**, 7 (2017).
- [43] N. Sowmya and H. C. Manjunatha, *Braz. J. Phys.* **49**, 874 (2019).
- [44] H. C. Manjunatha, K. N. Sridhar, and N. Sowmya, *Phys. Rev. C* **98**, 024308 (2018).
- [45] K. N. Sridhar, H. C. Manjunatha, and H. B. Ramalingam, *Phys. Rev. C* **98**, 064605 (2018).
- [46] N. Sowmya and H. C. Manjunatha, *Bulg. J. Phys.* **46**, 16 (2019).
- [47] N. Sowmya and H. C. Manjunatha, *Braz. J. Phys.* **50**, 317 (2020).
- [48] N. Sowmya and H. C. Manjunatha, *Phys. Part. Nucl. Lett.* **17**, 370 (2020).
- [49] H. C. Manjunatha, *Int. J. Mod. Phys. E* **25**, 1650074 (2016).
- [50] H. C. Manjunatha, N. Sowmya, K. N. Sridhar, and L. Seenappa, *J. Radiol. Nucl. Chem.* **314**, 991 (2017).
- [51] H. C. Manjunatha and N. Sowmya, *Int. J. Mod. Phys. E* **27**, 1850041 (2018).
- [52] M. G. Srinivas, H. C. Manjunatha, K. N. Sridhar, N. Sowmya, and A. C. Raj, *Nucl. Phys. A* **995**, 121689 (2020).
- [53] N. Sowmya, H. Manjunatha, N. Dhananjaya, and A. Nagaraja, *J. Radiol. Nucl. Chem.* **323**, 1347 (2020).
- [54] G. R. Sridhar, H. C. Manjunatha, N. Sowmya, P. S. Damodara Gupta, and H. B. Ramalingam, *Eur. Phys. J. Plus* **135**, 1 (2020).

- [55] H. C. Manjunatha and K. N. Sridhar, *Eur. Phys. J. A* **53**, 156 (2017).
- [56] H. C. Manjunatha and K. N. Sridhar, *Nucl. Phys. A* **975**, 136 (2018).
- [57] K. N. Sridhar, H. C. Manjunatha, and H. B. Ramalingam, *Nucl. Phys. A* **983**, 195 (2019).
- [58] H. C. Manjunatha and K. N. Sridhar, *Phys. Part. Nucl. Lett.* **16**, 647 (2019).
- [59] K. N. Sridhar, H. C. Manjunatha, and H. B. Ramalingam, *Braz. J. Phys.* **49**, 232 (2019).
- [60] N. Wang, K. Zhao, W. Scheid, and X. Wu, *Phys. Rev. C* **77**, 014603 (2008).
- [61] A. Dobrowolski, K. Pomorski, and J. Bartel, *Nucl. Phys. A* **729**, 713 (2003).
- [62] M. Liu, N. Wang, Z. Li, X. Wu, and E. Zhao, *Nucl. Phys. A* **768**, 80 (2006).
- [63] N. Wang, X. Wu, Z. Li, M. Liu, and W. Scheid, *Phys. Rev. C* **74**, 044604 (2006).
- [64] C. Wong, *Phys. Rev. Lett.* **31**, 766 (1973).
- [65] W. Reisdorf and M. Schädel, *Z. Phys. A: Hadrons Nucl.* **343**, 47 (1992).
- [66] V. I. Zagrebaev *et al.*, Nrv video project, http://nrv.jinr.ru/nrv/webnrv/evaporation_residue_theory/description/Decay%20of%20excited%20nuclei.pdf.
- [67] H. A. Kramers, *Physica* **7**, 284 (1940).
- [68] H. Manjunatha, *Indian J. Phys.* **92**, 507 (2018).
- [69] A. V. Ignatyuk, G. N. Smirenkin, and A. S. Tishin, *Sov. J. Nucl. Phys.* **21**, 485 (1975).
- [70] S. Cohen and W. J. Swiatecki, *Ann. Phys.* **22**, 406 (1963).
- [71] A. J. Sierk, *Phys. Rev. C* **33**, 2039 (1986).
- [72] W. D. Myers and W. J. Swiatecki, *Nucl. Phys.* **81**, 1 (1966).
- [73] R. du Rietz, E. Williams, D. J. Hinde, M. Dasgupta, M. Evers, C. J. Lin, D. H. Luong, C. Simenel, and A. Wakhle, *Phys. Rev. C* **88**, 054618 (2013).
- [74] S. Hofmann, F. Heßberger, D. Ackermann, G. Münzenberg, S. Antalic, P. Cagarda, B. Kindler, J. Kojouharova, M. Leino, B. Lommel *et al.*, *Eur. Phys. J. A: Hadrons Nucl.* **14**, 147 (2002).
- [75] K. Morita, K. Morimoto, D. Kaji, T. Akiyama, S.-i. Goto, H. Haba, E. Ideguchi, R. Kanungo, K. Katori, H. Koura *et al.*, *J. Phys. Soc. Jpn.* **73**, 2593 (2004).
- [76] Y. T. Oganessian, V. K. Utyonkov, Y. V. Lobanov, F. S. Abdullin, A. N. Polyakov, I. V. Shirokovsky, Y. S. Tsyganov, G. G. Gulbekian, S. L. Bogomolov, A. N. Mezentsev, S. Iliev, V. G. Subbotin, A. M. Sukhov, A. A. Voinov, G. V. Buklanov, K. Subotic, V. I. Zagrebaev, M. G. Itkis, J. B. Patin, K. J. Moody *et al.*, *Phys. Rev. C* **69**, 021601(R) (2004).
- [77] Y. T. Oganessian, F. S. Abdullin, P. D. Bailey, D. E. Benker, M. E. Bennett, S. N. Dmitriev, J. G. Ezold, J. H. Hamilton, R. A. Henderson, M. G. Itkis, Y. V. Lobanov, A. N. Mezentsev, K. J. Moody, S. L. Nelson, A. N. Polyakov, C. E. Porter, A. V. Ramayya, F. D. Riley, J. B. Roberto, M. A. Ryabinin *et al.*, *Phys. Rev. Lett.* **104**, 142502 (2010).
- [78] Y. T. Oganessian, F. S. Abdullin, C. Alexander, J. Binder, R. A. Boll, S. N. Dmitriev, J. Ezold, K. Felker, J. M. Gostic, R. K. Grzywacz, J. H. Hamilton, R. A. Henderson, M. G. Itkis, K. Miernik, D. Miller, K. J. Moody, A. N. Polyakov, A. V. Ramayya, J. B. Roberto, M. A. Ryabinin *et al.*, *Phys. Rev. Lett.* **109**, 162501 (2012).
- [79] V. S. Ramamurthy, S. S. Kapoor, R. K. Choudhury, A. Saxena, D. M. Nadkarni, A. K. Mohanty, B. K. Nayak, S. V. Sastry, S. Kailas, A. Chatterjee, P. Singh, and A. Navin, *Phys. Rev. Lett.* **65**, 25 (1990).
- [80] B. R. Behera, S. Jena, M. Satpathy, S. Kailas, K. Mahata, A. Shrivastava, A. Chatterjee, S. Roy, P. Basu, M. K. Sharan, and S. K. Datta, *Phys. Rev. C* **64**, 041602(R) (2001).
- [81] J. Blocki, H. Feldmeier, and W. Swiatecki, *Nucl. Phys. A* **459**, 145 (1986).
- [82] W. Loveland, *Phys. Rev. C* **76**, 014612 (2007).